PHYSICAL REVIEW D **72,** 034037 (2005)

Charmless decays $B \to \pi\pi$, πK and KK in broken SU(3) symmetry

Yue-Liang Wu*
Institute of Theoretical Physics, CAS, Beijing, 100080, China

Yu-Feng Zhou†
Institute for Physics, Dortmund University, D-44221, Dortmund, Germany
(Received 14 March 2005; published 31 August 2005)

Charmless B decay modes $B \to \pi\pi$, πK and KK are systematically investigated with and without flavor SU(3) symmetry. Independent analyses on $\pi\pi$ and πK modes *both* favor a large ratio between color-suppressed tree (C) and tree (T) diagram, which suggests that they are more likely to originate from long distance effects. The sizes of QCD penguin diagrams extracted individually from $\pi\pi$, πK and KK modes are found to follow a pattern of SU(3) breaking in agreement with the naive factorization estimates. Global fits to these modes are done under various scenarios of SU(3) relations. The results show good determinations of weak phase γ in consistency with the standard model (SM), but a large electroweak penguin ($P_{\rm EW}$) relative to $T + C$ with a large relative strong phase is favored, which requires a big enhancement of color-suppressed electroweak penguin ($P^C_{\rm EW}$) compatible in size but destructively interfering with $P_{\rm EW}$ within the SM, or implies new physics. The possibilities of sizable contributions from nonfactorizable diagrams such as W exchange (E), annihilation (A), and penguin-annihilation diagrams (P_A) are investigated. The implications to the branching ratios and CP violations in KK modes are discussed.

DOI: 10.1103/PhysRevD.72.034037 PACS numbers: 13.25.Hw, 11.30.Er, 11.30.Hv

I. INTRODUCTION

In recent years, the two B factories have succeeded in steadily improving the measurements of hadronic charmless B decays. At present, all the branching ratios of $B \to \pi\pi$ and πK modes have been measured with good accuracy. The large direct CP violations have also been established in $\pi^+\pi^-$ and π^+K^- modes [1]. Their implications have been reported in a recent short paper [2]. It has been shown that the weak phase γ can well be determined to be consistent with the standard model; it prefers a relative large electroweak penguin with a large strong phase and also favors an enhanced color-suppressed tree diagram. In this longer paper, we shall provide a more detailed analysis including subleading diagrams and their implications to KK modes as well as paying attention to SU(3) broken effects.

It is of interest to note that the signs of the direct CP violations, if confirmed by the future experiments, would agree with the results from the perturbative QCD approach [3,4] while possessing a challenge to the naive factorization [5,6] and QCD factorization calculations [7–10]. These impressive new results have triggered a large amount of theoretical efforts to understand the strong interaction dynamics of those decays [11–15], extract the weak phases in the Cabbibo-Kobayashi-Maskawa (CKM) matrix [16,17], and explore new physics [18–24].

Making use of the flavor topology of the decay amplitudes and the approximate flavor SU(3) symmetry, one can describe those decay modes in terms of several independent quark flavor flow diagrams, such as the tree diagram ($\mathcal{T}$), the color-suppressed tree diagram (C), the QCD penguin diagram ($\mathcal{P}$), the electroweak penguin diagram ($\mathcal{P}_{\rm EW}$), and the color-suppressed electroweak penguin diagram ($\mathcal{P}^C_{\rm EW}$), etc. It then follows from the hierarchies of the Wilson coefficients and the CKM matrix elements that the $B \to \pi\pi$ modes are $\mathcal{T}$ dominant while the $B \to \pi K$ modes are $\mathcal{P}$ dominant. Since C is color suppressed, one expects that the hierarchical structures among those decays should be

$$2\mathrm{Br}(\pi^0\pi^0) \ll \mathrm{Br}(\pi^+\pi^-) \approx 2\mathrm{Br}(\pi^-\pi^0), \tag{1}$$

and

$$\mathrm{Br}(\pi^+K^-) \simeq \mathrm{Br}(\pi^-\bar{K}^0) \simeq 2\mathrm{Br}(\pi^0\bar{K}^0) \simeq 2\mathrm{Br}(\pi^0K^-), \tag{2}$$

respectively.

Note that the above relations follow from a purely short distance diagrammatic description which could be misleading in the presence of large final state interactions (FSIs) [25–27]. At present, they are not favored by the experiments. The current world average data [1,28] listed in Table I show big enhancements of $\mathrm{Br}(\pi^0\pi^0)$ and $\mathrm{Br}(\pi^-\pi^0)$ relative to $\mathrm{Br}(\pi^+\pi^-)$ and a suppression of $\mathrm{Br}(\pi^+K^-)$ relative to $2\mathrm{Br}(\pi^0\bar{K}^0)$ and $\mathrm{Br}(\pi^-\bar{K}^0)$. The numerical values of these relative ratios are given by [20]

*Email address: ylwu@itp.ac.cn
†Email address: zhou@zylon.physik.uni-dortmund.de

TABLE I. The latest world averaged data of charmless B decays [1,28].

Modes	Br($\times 10^{-6}$)	a_{CP}	S
$\pi^+\pi^-$	4.6 ± 0.4	0.37 ± 0.11	-0.61 ± 0.14
$\pi^0\pi^0$	1.51 ± 0.28	0.28 ± 0.39	
$\pi^-\pi^0$	5.5 ± 0.6	-0.02 ± 0.07	
π^+K^-	18.2 ± 0.8	-0.11 ± 0.02	
$\pi^0\bar{K}^0$ (K_S)	11.5 ± 1.0	-0.09 ± 0.14	$(+0.34 \pm 0.28)$
$\pi^-\bar{K}^0$	24.1 ± 1.3	-0.02 ± 0.034	
π^0K^-	12.1 ± 0.8	0.04 ± 0.04	
K^+K^-			
$K^0\bar{K}^0$	$1.19^{+0.42}_{-0.37}$		
$K^-\bar{K}^0$	$<2.4(1.45^{+0.53}_{-0.46})$		

$$R_{+-} = 2\frac{\mathrm{Br}(\pi^-\pi^0)}{\mathrm{Br}(\pi^+\pi^-)}\cdot\frac{\tau_{B^0}}{\tau_{B^+}} = 2.2 \pm 0.31,$$
$$R_{00} = 2\frac{\mathrm{Br}(\pi^0\pi^0)}{\mathrm{Br}(\pi^+\pi^-)} = 0.67 \pm 0.14, \tag{3}$$

and also

$$R_n = \frac{\mathrm{Br}(\pi^+K^-)}{2\mathrm{Br}(\pi^0\bar{K}^0)} = 0.79 \pm 0.08,$$
$$R = \frac{\mathrm{Br}(\pi^+K^-)}{\mathrm{Br}(\pi^-\bar{K}^0)}\cdot\frac{\tau_{B^+}}{\tau_{B^0}} = 0.82 \pm 0.06, \tag{4}$$
$$R_2 = \frac{\mathrm{Br}(\pi^+K^-)}{2\mathrm{Br}(\pi^0K^-)}\cdot\frac{\tau_{B^+}}{\tau_{B^0}} = 0.81 \pm 0.06.$$

The above five ratios characterize the puzzling patterns of the latest data and may provide insights on the strong dynamics of heavy quark decays or possible new physics beyond the standard model (SM).

The large value of R_{00} forces the C to be large, which is a challenge to theory. Various ways to explain large R_{00} with reasonable values of $C/\mathcal{T}$ involve an enhanced W-exchange diagram ($\mathcal{E}$), a large QCD penguin contribution corresponds to the u-quark loop or FSIs which involves $DD_{(s)}$ intermediate states and quasielastic mixing between $\pi^+\pi^-$ and $\pi^0\pi^0$ modes [14]. The recent soft colinear effective theory (SCET) calculations also supported a large $C/\mathcal{T}$ [29]. Note that the $\pi\pi$ and πK modes differ in flavor topological structure while FSIs are flavor blind; the two kind of effects can in principle be distinguished by a separated study of these two sets. FSI will lead to large C in all decays modes. Furthermore, it should enhance $\mathcal{P}^C_{\mathrm{EW}}$ relative to $\mathcal{P}_{\mathrm{EW}}$ in a similar manner.

In the πK modes, it is well known that the suppression of R_n is more relevant to the electroweak penguin sector. As in πK modes $\mathcal{T}$ and C are greatly suppressed by small CKM matrix elements. In the SM, from the isospin structure of the effective Hamiltonian, the ratios between electroweak penguin and tree diagrams are fixed through [30–34]

$$R^{\mathrm{SM}}_{\mathrm{EW}} = \frac{P_{\mathrm{EW}} + P^C_{\mathrm{EW}}}{T + C} = -\frac{3}{2}\cdot\frac{C_9 + C_{10}}{C_1 + C_2}$$
$$= (1.35 \pm 0.12) \times 10^{-2}, \tag{5}$$

for $\pi\pi$ modes. T, C, P_{EW}, and P^C_{EW} are diagrams with CKM matrix elements factorized out which will be discussed in detail below. C_is stand for the short distance Wilson coefficients at the scale of $\mu \simeq m_b$. This relation is free from hadronic uncertainties and survives under elastic FSIs and inelastic FSIs through low isospin states such as $B \to DD_s \to \pi\pi(K)$. It also predicts the direct CP violation in $\pi^-\pi^0$ modes to be vanishing. Using flavor SU(3) symmetry, this relation also holds for πK modes. Thus it can directly confront the experiments and allows us to explore the new physics in hadronic charmless B decays. It is of interest that the charmless B decay data indeed imply the violation of Eq. (5). The possibility of larger isospin $I = 2(3/2)$ amplitudes violating Eq. (5) in $\pi\pi(\pi K)$ modes was found in Ref. [35] and recently discussed in Refs. [2,18–20,36–39] with updated data. In a recent analysis, an enhancement of a factor of 2 was obtained through a direct global χ^2 analysis using flavor SU(3) symmetry [2].

Although it is too early to draw any robust conclusion, it motivates us to take a closer look at the electroweak penguin sector within and beyond the SM. Note that in these analyses on large P_{EW}, the effects of P^C_{EW} are often assumed to be small, which is conceptually not appropriate as P^C_{EW} is directly involved in Eq. (5). Furthermore, it provides a cancellation to the low isospin $I = 0(1/2)$ part of P_{EW}. Thus its effects could be significant.

The suppression of R may require significant contributions from subleading diagrams such as annihilation diagram $\mathcal{A}$ or color-suppressed electroweak penguin diagram $\mathcal{P}^C_{\mathrm{EW}}$. Considering the fact that $\mathcal{A}$ contributes to $\pi^-\bar{K}^0$ and π^0K^- in the same way, namely, they have the same $\mathcal{A} - \mathcal{P}$ interference, one expects that an enhancement of $\mathcal{A}$ with an appropriate strong phase can suppress simultaneously R and R_2 while their effects would cancel to some extent in their ratio. The current data give

$$R_3 = \frac{2\mathrm{Br}(\pi^0K^-)}{\mathrm{Br}(\pi^-\bar{K}^0)} = 1.0 \pm 0.08, \tag{6}$$

which agrees well with this conjecture. However an enhancement of $\mathcal{A}$ will lead to significant consequences to KK modes, especially $K^-\bar{K}^0$, as it is not suppressed by the CKM matrix element like in the πK modes. It is expected that a strong constraint on $\mathcal{A}$ will be found once this decay mode is experimentally observed.

There already exists a number of global χ^2 analyses on $B \to \pi\pi, \pi K$ and KK systems based on flavor SU(3) symmetry [12,35,40–44]. But to trace back the origins of the above mentioned $\pi\pi$ and πK puzzles, *separate* χ^2 analyses are urgently needed. Furthermore, the SU(3) breaking scheme dependences are not carefully examined

in the previous analyses, which may lead to different results in the literature. Finally, the contributions from subleading diagrams such as $\mathcal{P}^C_{\rm EW}$, $\mathcal{E}$, $\mathcal{A}$, and penguin-induced annihilation diagram $\mathcal{P}_A$ which could play important roles in understanding the current data are often neglected.

The purpose of the present paper is to make an up to date investigation on charmless B decays, following a strategy by first applying the χ^2 analysis on $\pi\pi$, πK, and KK modes separately, then connecting them through flavor SU(3) symmetry, and discussing the SU(3) breaking scheme dependency. After obtaining reasonable values of the dominant amplitudes, we then discuss their implications to KK modes with subleading diagrams such as $\mathcal{P}^C_{\rm EW}$, $\mathcal{E}$, $\mathcal{A}$, $\mathcal{P}_A$, etc.

Our main observations are the following:

(i) Independent fits on $\pi\pi$ and πK modes without SU(3) symmetry both favor a large ratio between color-suppressed tree ($\mathcal{C}$) and tree ($\mathcal{T}$) diagrams, which disfavors the explanation of large nonfactorizable W-exchange diagrams ($\mathcal{E}$). The extracted QCD penguin diagrams from $\pi\pi$, πK, and KK show a clear signal of SU(3) breaking and the breaking pattern is in agreement with naive factorization.

(ii) Global fits for $\pi\pi$, πK, and KK modes show good determinations of weak phase γ in agreement with the standard model and prefer a larger electroweak penguin ($\mathcal{P}_{\rm EW}$) relative to $\mathcal{T} + \mathcal{C}$ with a large strong phase when $P^C_{\rm EW}$ is neglected. The results are found stable among various SU(3) breaking schemes. The current data favor a SU(3) breaking scheme in which all the amplitudes for πK are greater by a factor of f_K/f_π motivated from factorization.

(iii) An enhancement of $\mathcal{P}^C_{\rm EW}$ with destructive interference to $P_{\rm EW}$ provides an alternative explanation to the small R_n within the SM. The suppression of R can be partially explained by an enhanced annihilation diagram $\mathcal{A}$. The $\mathcal{P}_A$ provides a source of SU(3) breaking in strong phases.

(iv) The subleading diagrams may lead to significant CP violations in KK modes. For a typical value of $\mathcal{A}$ and $\mathcal{P}$, the direct CP violation in $K^-\bar{K}^0$ can reach $\sim$0.4.

This paper is organized as follows. In Sec. II, the basic formulas for diagrammatic decomposition are presented. In III, we extract the parameters such as weak phase γ and the decay amplitudes from $\pi\pi$, πK, and KK modes separately. In Sec. IV, we combine them in three different scenarios of SU(3) symmetry. One is that all the amplitudes in πK modes are rescaled by a factor of f_K/f_π motivated from the native factorization. An other one is that only the tree diagrams are rescaled by this factor while the rest of the amplitudes remain the same in the SU(3) limit. The last one is the strict SU(3) limit. In Sec. V, we consider the contributions from various subleading diagrams and extract their typical values. In Sec. VI, the implications to the KK modes are discussed. The possibility of finding large direct CP violations is indicated. We conclude in Sec. VII.

II. DIAGRAMMATIC DESCRIPTION

We use the following definitions for branching ratios and direct CP violations:

$$\mathrm{Br} = \frac{1}{2}\tau(|\bar{\mathcal{A}}|^2 + |\mathcal{A}|^2), \qquad a_{CP} = \frac{|\bar{\mathcal{A}}|^2 - |\mathcal{A}|^2}{|\bar{\mathcal{A}}|^2 + |\mathcal{A}|^2}, \tag{7}$$

where $\mathcal{A}(\bar{\mathcal{A}})$ stands for the $B^0(\bar{B})$ or the $B^+(B^-)$ decay amplitude. τ is a phase space factor, $\tau = 1$ for neutral final states, and $\tau = \tau_{B^+}/\tau_{B^0} = 1.086 \pm 0.017$ for charged final states. The mixing induced CP violation parameters S and C are introduced through the time-dependent decay rate difference

$$\begin{aligned} a_{CP}(t) &= \frac{\Gamma(\bar{B}^0 \to f_{CP}) - \Gamma(B^0 \to f_{CP})}{\Gamma(\bar{B}^0 \to f_{CP}) + \Gamma(B^0 \to f_{CP})} \\ &= S \cdot \sin(\Delta m_B \cdot t) - C \cdot \cos(\Delta m_B \cdot t), \end{aligned} \tag{8}$$

with f_{CP} denoting final states with definite CP parities. Δm_B is the neutral B meson mass difference. The two parameters can be written as

$$S = \frac{2\mathrm{Im}\lambda}{1 + |\lambda|^2}, \qquad C = \frac{1 - |\lambda|^2}{1 + |\lambda|^2} = -a_{CP}, \tag{9}$$

with

$$\lambda = e^{-2i\beta}\frac{\bar{\mathcal{A}}}{\mathcal{A}} \tag{10}$$

in the SM.

Using the phase definitions of $B^- = (-\bar{u}b)$, $\bar{B}^0 = (\bar{d}b)$, $K^- = (-\bar{u}s)$, $\bar{K}^0 = (\bar{d}s)$ and $\pi^+ = (u\bar{d})$, $\pi^0 = (d\bar{d} - u\bar{u})/2$, $\pi^- = (-\bar{u}d)$, one arrives at the following diagrammatic decompositions for $\pi\pi$ modes [45–47]:

$$\begin{aligned} \bar{\mathcal{A}}(\pi^+\pi^-) &= -\left(\mathcal{T} + \mathcal{E} + \mathcal{P} + \mathcal{P}_A + \frac{2}{3}\mathcal{P}^C_{\rm EW}\right), \\ \bar{\mathcal{A}}(\pi^0\pi^0) &= -\frac{1}{\sqrt{2}}\left(\mathcal{C} - \mathcal{E} - \mathcal{P} - \mathcal{P}_A + \mathcal{P}_{\rm EW} + \frac{1}{3}\mathcal{P}^C_{\rm EW}\right), \\ \bar{\mathcal{A}}(\pi^0\pi^-) &= -\frac{1}{\sqrt{2}}(\mathcal{T} + \mathcal{C} + \mathcal{P}_{\rm EW} + \mathcal{P}^C_{\rm EW}). \end{aligned} \tag{11}$$

Similarly, the πK modes are given by

$$\bar{\mathcal{A}}(\pi^+K^-) = -\left(\mathcal{T}' + \mathcal{P}' + \frac{2}{3}\mathcal{P}^{C'}_{\rm EW}\right),$$
$$\bar{\mathcal{A}}(\pi^0\overline{K}^0) = -\frac{1}{\sqrt{2}}\left(C' - \mathcal{P}' + \mathcal{P}'_{\rm EW} + \frac{1}{3}\mathcal{P}^{C'}_{\rm EW}\right),$$
$$\bar{\mathcal{A}}(\pi^-\overline{K}^0) = \mathcal{A}' + \mathcal{P}' - \frac{1}{3}\mathcal{P}^{C'}_{\rm EW},$$
$$\bar{\mathcal{A}}(\pi^0K^-) = -\frac{1}{\sqrt{2}}\left(\mathcal{T}' + C' + \mathcal{A}' + \mathcal{P}' + \mathcal{P}'_{\rm EW} + \frac{2}{3}\mathcal{P}^{C'}_{\rm EW}\right). \quad (12)$$

The amplitudes for πK modes are marked by a prime, which equal the unprimed ones for $\pi\pi$ modes in the flavor SU(3) limit. The KK modes are given by

$$\bar{\mathcal{A}}(K^+K^-) = -(\mathcal{E}'' + \mathcal{P}''_A),$$
$$\bar{\mathcal{A}}(K^0\bar{K}^0) = \mathcal{P}'' - \frac{1}{3}\mathcal{P}^{C''}_{\rm EW} + \mathcal{P}''_A, \quad (13)$$
$$\bar{\mathcal{A}}(K^-\bar{K}^0) = \mathcal{P}'' - \frac{1}{3}\mathcal{P}^{C''}_{\rm EW} + \mathcal{A}'',$$

where the subleading diagrams such as the color-suppressed electroweak penguin ($\mathcal{P}^C_{\rm EW}$), the W-exchange diagram ($\mathcal{E}$), the annihilation diagram $\mathcal{A}$, and the penguin-induced annihilation diagram ($\mathcal{P}_A$) are included. In the above formulas, the penguin exchange diagrams ($\mathcal{P}_E$) are absorbed into penguin diagrams and the electroweak and color-suppressed electroweak penguin exchange diagrams are neglected.

We start with independent analyses on $\pi\pi$, πK, and KK modes. In the first step, all subleading diagrams such as $\mathcal{P}^C_{\rm EW}$, $\mathcal{E}$, $\mathcal{P}_A$, and $\mathcal{A}$ are switched off for the reason of simplicity. Their effects will be investigated in detail in Secs. IV and V. To consistently include the experimental errors of the data, the χ^2 method is adopted for extracting the decay amplitudes. The definition of χ^2 reads

$$\chi^2 = \sum_i \left(\frac{f^{\rm theo}(\alpha_j)_i - f_i^{\rm exp}}{\sigma_i}\right)^2, \quad (14)$$

where $f_i^{\rm theo}$ are the theoretical values of observables $f_i (i = 1, m)$ and $\alpha_j (j = 1, n)$ are the to-be-determined parameters. $f_i^{\rm exp}$ and σ_i are the experimental central values and errors. The best fit of the parameters corresponds to the minimum of the χ^2 function which satisfies a χ^2 distribution with degree of freedom (d.o.f.) $m - n$. For the experimental data we take the values listed in Table I which are the weighted average of the CLEO, *BABAR*, and Belle Collaboration results [28]. Other major parameters used in the fits involve the CKM matrix elements of V_{ub} [48,49] and V_{cb} [50]. In the numerical calculations we take the following values [28]:

$$V_{cb} = 0.04 \pm 0.02, \qquad V_{ub} = (3.9 \pm 0.68) \times 10^{-3}, \quad (15)$$

and the SM value of [51,52]

$$\sin 2\beta = 0.73 \pm 0.037. \quad (16)$$

All the Brs are written in units of 10^{-6}, and the angles are in gradient and arranged in the range $(-\pi, +\pi)$.

III. ANALYSIS WITHOUT FLAVOR SU(3) SYMMETRY

A. $\pi\pi$ modes

The hierarchies in the decay amplitudes are controlled by both the Wilson coefficients and the CKM matrix elements. As the sizes of the CKM matrix elements are better known, it is helpful to factorize them out so that all the hadronic amplitudes in $\pi\pi$, πK, and KK etc. have the same hierarchical structure. Thus we shall use the following parametrizations for $\pi\pi$ modes:

$$\bar{\mathcal{A}}(\pi^+\pi^-) = -\left[\lambda_u\left(T + E - P - P_A - \frac{2}{3}P^C_{\rm EW}\right) - \lambda_c\left(P + P_A + \frac{2}{3}P^C_{\rm EW}\right)\right],$$
$$\bar{\mathcal{A}}(\pi^0\pi^0) = -\frac{1}{\sqrt{2}}\left[\lambda_u\left(C - E + P + P_A - P_{\rm EW} - \frac{1}{3}P^C_{\rm EW}\right) - \lambda_c\left(-P - P_A + P_{\rm EW} + \frac{1}{3}P^C_{\rm EW}\right)\right], \quad (17)$$
$$\bar{\mathcal{A}}(\pi^0\pi^-) = -\frac{1}{\sqrt{2}}[\lambda_u(T + C - P_{\rm EW} - P^C_{\rm EW}) - \lambda_c(P_{\rm EW} + P^C_{\rm EW})],$$

with $\lambda_u = V_{ub}V^*_{ud} = A\lambda^3(\rho - i\eta)(1 - \lambda^2/2)$, and $\lambda_c = V_{cb}V^*_{cd} = -A\lambda^3$. Throughout the present paper, we shall assume the t-quark dominance in penguin-type diagrams. In general a penguin diagram can be written as

$$\mathcal{P} = \lambda_u P_u + \lambda_c P_c + \lambda_t P_t = -\lambda_u P_{tu} - \lambda_c P_{tc}, \quad (18)$$

where $P_{tu} = P_t - P_u$ and $P_{tc} = P_t - P_c$. The t-quark dominance in the Wilson coefficient then leads to $P_t \gg P_c \gg P_u$ and

$$P_{tu} \simeq P_{tc} \simeq P_t \equiv P. \quad (19)$$

Note that in the presence of a large charming penguin [29,53–56], P_{tc} could differ from P. This effect can be effectively absorbed into inelastic FSIs and will not be discussed in detail here.

From the isospin structure of the low energy effective Hamiltonian, the sum $T + C$ and $P_{\rm EW} + P^C_{\rm EW}$ have both isospin $I = 2$. It is then helpful to define

$$\hat{T} = T + C, \qquad \hat{P}_{\rm EW} = P_{\rm EW} + P^C_{\rm EW}. \quad (20)$$

The ratio $R_{\rm EW}^{\rm SM}$ is just the ratio of the isospin $I = 2$ part between electroweak penguin and tree diagrams.

In the naive factorization approach [5,6], these amplitudes have the following typical values:

$$T = 0.9\text{–}1.1, \qquad C = -0.33\text{–}0.25, \qquad P \simeq 0.1, \\ P_{\rm EW} = 0.013\text{–}0.015, \qquad P_{\rm EW}^C = -0.0023\text{–}0.003. \tag{21}$$

All the amplitudes are almost real. The ranges of the parameters correspond to the effective number of color N_C ranging from 2 to infinity. In the factorization approach, the rescaled amplitudes satisfy a hierarchy of

$$|T| \gg |P| \gg |P_{\rm EW}|, |P_{\rm EW}^C|, \tag{22}$$

which holds for all primed and double-primed amplitudes in πK and KK modes.

Including the time-dependent CP asymmetry, the $\pi\pi$ modes provide seven data points. A direct fit to the data gives the following best fits corresponding to a local minimum of χ^2 function:

$$|T| = 0.53^{+0.036}_{-0.031}, \qquad |C| = 0.42^{+0.081}_{-0.11}, \\ \delta_C = -0.84^{+0.57}_{-0.41}, \qquad |P| = 0.099^{+0.038}_{-0.045}, \\ \delta_P = -0.55^{+0.27}_{-0.73}, \qquad \gamma = 1.1^{+0.26}_{-0.29}, \tag{23}$$

with $\chi^2_{\rm min}/{\rm d.o.f.} = 0.17/1$, where $P_{\rm EW}$ is fixed relative to $\hat{T}$ through Eq. (5). The above result shows that

(i) The $\pi\pi$ data prefer a large $|C/T| = 0.8 \pm 0.2$, which is in contradiction with the factorization based estimation. This is not new, however; a large relative strong phase of $\delta_C = -0.84^{+0.57}_{-0.41}$ is also favored. Note that the recent SCET calculation which includes charming penguin effects prefers that ${\rm Im}(C/T)$ should be vanishing at leading order [29]. In the present $\pi\pi$ fit the charming penguin amplitude is not included. The considerable uncertainties in the present data prevent us from drawing a robust conclusion on the phase of C/T. The situation will be improved when more precise data are available in the near future. The large $|C|$ and its strong phase δ_C are required by the observed two ratios in Eq. (3). In the following figure (Fig. 1), the dependences of the ratios with $|C/T|$ and δ_C are given. For illustration purpose, we fix other parameters to be $|T| = 0.53$, $|P| = 0.1$, $\delta_P = -0.55$, and $\gamma = 1.1$, corresponding to their best fits.

It follows from Fig. 1 that both R_{+-} and R_{00} prefer a large $|C/T|$ around 0.8. There is very little dependence on δ_C for R_{00}. However, the large strong phase of $\delta_C \simeq -1.0$ is required by R_{+-}, namely, by the interference between T and C in the $\pi^-\pi^0$ mode.

(ii) The determination of γ is in agreement with the SM fit. However, in the $\pi\pi$ system, there could be multiple solutions [17,57]. The χ^2 curve as a function of γ is given in Fig. 2, which also indicates a local minimum of χ^2 close to $\gamma = 0.23$. But the other corresponding best fitted parameters are $|T| \simeq 0.3$, $|C| \simeq 0.84$, $\delta_C \simeq -1.7$, and $|P| \simeq 0.36$ which looks unreasonable as they favor $|C| \gg |T|$ and $|T| \simeq |P|$. To get rid of the multiple solutions, one may include the πK modes via flavor SU(3) symmetry. The simplest way is to include π^+K^- mode only, as was done in Ref. [2]. The twofold ambiguity in γ can be easily lifted.

(iii) The value of $|P| \simeq 0.1$ agrees well with the naive factorization estimate in Eq. (21) while T is suppressed. The enhancement of C and the suppression of T implies that there could be a mixing between a diagram and its color-suppressed counterpart. For $\pi\pi$ modes, it may be due to large FSI through $B \to \pi^+\pi^-(\pi^0\pi^0) \to \pi^0\pi^0(\pi^+\pi^-)$. A recent calculation based on one particle exchange model indeed supports this conjecture [14]. Such a mixing may also apply to $D^0\pi^0$ and $\rho^0\pi^0$ modes.

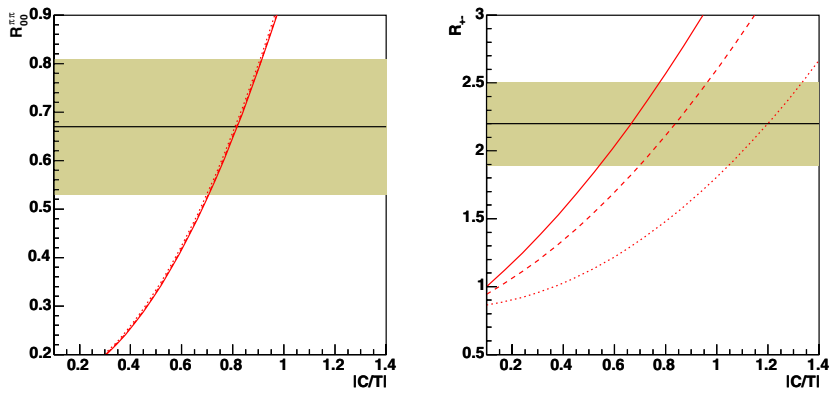

FIG. 1 (color online). R_{00} and R_{+-} as functions of $|C/T|$ with a different value of δ_C. The three curves correspond to $\delta_C = -0.5$, -1.0, and -1.5, respectively. The shadowed bands are the experimentally 1σ allowed ranges. The other parameters are fixed at their best-fit value in Eq. (23).

B. πK modes

The amplitudes of πK modes are written in a similar way

$$\begin{aligned}
\bar{\mathcal{A}}(\pi^+K^-) &= -\Big[\lambda_u^s\Big(T' - P' - \frac{2}{3}P_{\rm EW}^{C'}\Big) - \lambda_c^s\Big(P' + \frac{2}{3}P_{\rm EW}^{C'}\Big)\Big],\\
\bar{\mathcal{A}}(\pi^0\overline{K}^0) &= -\frac{1}{\sqrt{2}}\Big[\lambda_u^s\Big(C' + P' - P'_{\rm EW} - \frac{1}{3}P_{\rm EW}^{C'}\Big) - \lambda_c^s\Big(-P' + P'_{\rm EW} + \frac{1}{3}P_{\rm EW}^{C'}\Big)\Big],\\
\bar{\mathcal{A}}(\pi^-\overline{K}^0) &= \lambda_u^s\Big(A' - P' + \frac{1}{3}P_{\rm EW}^{C'}\Big) - \lambda_c^s\Big(P' - \frac{1}{3}P_{\rm EW}^{C'}\Big),\\
\bar{\mathcal{A}}(\pi^0K^-) &= -\frac{1}{\sqrt{2}}\Big[\lambda_u^s\Big(T' + C' + A' - P' - P'_{\rm EW} - \frac{2}{3}P_{\rm EW}^{C'}\Big) - \lambda_c^s\Big(P' + P'_{\rm EW} + \frac{2}{3}P_{\rm EW}^{C'}\Big)\Big],
\end{aligned} \tag{24}$$

with $\lambda_u^s = V_{ub}V_{us}^* = A\lambda^4(\rho - i\eta)$, and $\lambda_c^s = V_{cb}V_{cs}^* = A\lambda^2(1-\lambda^2/2)$. Note that in the πK modes $|\lambda_u^s|$ is much smaller than $|\lambda_c^s|$, $|\lambda_u^s/\lambda_c^s| \simeq 0.02$. The suppression of the tree-penguin interference and the limited accuracy of the present data make it less effective to extract the weak phase γ from πK modes at the present stage. Thus if one considers πK modes alone, it is more useful to take γ as known from the global SM fit to explore the other hadronic decay amplitudes. Taking the SM value of $\gamma = 1.08^{+0.17}_{-0.21}$ as input and also fixing the $P'_{\rm EW}$ with the SM relation of Eq. (5), one finds the following solution:

$$\begin{aligned}
&|T'| = 1.54^{+0.61}_{-0.38}, \qquad |C'| = 2.7^{+0.61}_{-0.7},\\
&\delta_{C'} = 3.1 \pm 0.11, \qquad |P'| = 0.12 \pm 0.0023,\\
&\delta_{P'} = -0.2^{+0.07}_{-0.12},
\end{aligned} \tag{25}$$

with a χ^2/d.o.f. $= 2.49/4$. From the above result, one arrives at the following observations:

(i) The πK data favor both large T' and C' with an even larger ratio of $|C'/T'| = 1.75 \pm 0.7$. Although the errors are considerably large, it is evident that a large $|C'/T'| \simeq \mathcal{O}(1)$ is also favored in πK modes. A similar observation was made in Ref. [58] where no error estimation was given. The large $|C'/T'|$ is due to the suppression of R_n from unity; in Fig. 3 the value of R_n as a function of $|C'/T'|$ is plotted, and one sees that in general, a large $|C'/T'|$ with a large relative strong phase $\delta_{C'} \simeq 2$ can lead to the reduction of the ratio R_n.

(ii) P' is well determined which is about 20% larger than P, in good agreement with the factorization based estimation that $P'/P \simeq f_K/f_\pi \simeq 1.28$.

(iii) A relatively larger χ^2/d.o.f. in the πK fit indicates larger inconsistency with the data in comparison with that for $\pi\pi$ modes . The sources of inconsistency mainly come from Br(π^+K^-) and Br$(\pi^0\bar{K}^0)$ and also $S(\pi^0K_S)$. The best fit prefers a larger value of $R_n \simeq 0.9$ and a very small $S(\pi^0K_S) \simeq -0.02$.

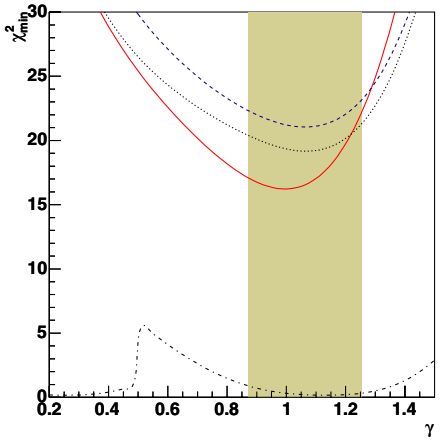

FIG. 2 (color online). $\chi^2_{\rm min}$ as functions of weak phase γ. The three upper curves correspond to the three fits in Table II. The solid, dashed, and dotted curves correspond to scenarios A, B, and C, respectively. The lower curve (dot-dashed) corresponds to the fit only to $\pi\pi$ modes in Eq. (23). The shadowed band is the allowed range from the global SM fit.

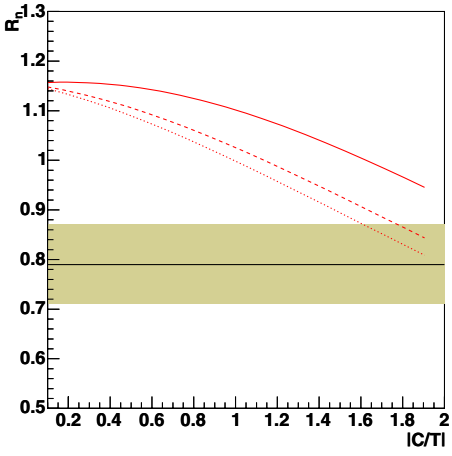

FIG. 3 (color online). R_n as functions of $|C'/T'|$ with a different value of $\delta_{C'}$. The three curves correspond to $\delta_{C'} = 1.0$, 2.0, and 3.0, respectively. The shadowed band is the experimentally 1σ allowed range.

An alternative way to achieve at a smaller R_n is to allow $P_{\rm EW}$ to be larger, which needs new physics effects beyond the SM. Taking $P_{\rm EW}$ to be free, one finds

$$\begin{aligned} |T'| &= 2.75^{+1.12}_{-1.38}, \qquad |C'| = 1.31^{+0.71}_{-0.75}, \\ \delta_{C'} &= 2.76 \pm 0.28, \qquad |P'| = 0.12 \pm 0.0023, \\ \delta_{P'} &= -0.08^{+0.02}_{-0.08}, \qquad |P'_{\rm EW}| = 0.048 \pm 0.02, \\ \delta_{P'_{\rm EW}} &= 1.44^{+0.08}_{-0.13}, \end{aligned} \tag{26}$$

with $\chi^2/\text{d.o.f.} = 0.4/2$. Indeed, one sees that a large $P'_{\rm EW}$ is favored by the πK data with $|P'_{\rm EW}/(T' + C')| = 0.04 \pm 0.04$. Once $P'_{\rm EW}$ is increasing, the ratio of C'/T' decreases. It seems to be a promising way to restore a reasonable value of C'/T'. However, it only holds for πK modes. Furthermore, the uncertainties are too large to prevent us to draw any robust conclusion. The precisions can be improved significantly by making use of the whole charmless B decay data connected by flavor SU(3) symmetry.

It is more difficult to explain the suppression of R in $\pi^+ K^-$ and $\pi^- \bar{K}^0$ modes, as both C and $P_{\rm EW}$ are absent. If the puzzle of R has to be taken seriously, one needs an enhancement of either A or $P^C_{\rm EW}$. This possibility will be discussed in Secs. IV and V.

C. KK modes

For the KK modes, currently only the $K^0\bar{K}^0$ mode has been observed. The decay amplitude is given by

$$\begin{aligned} \bar{\mathcal{A}}(K^0\bar{K}^0) = \lambda_u &\left(-P'' + \frac{1}{3}P^{C''}_{\rm EW} - P''_A\right) \\ &- \lambda_c\left(P'' - \frac{1}{3}P^{C''}_{\rm EW} + P''_A\right), \end{aligned} \tag{27}$$

which is dominated by the QCD penguin (through $b \to d$). Neglecting small subleading diagrams $P^C_{\rm EW}$ and P_A, one can directly extract the amplitude of the penguin from the data

$$|P''| = 0.2^{+0.4}_{-0.3}, \tag{28}$$

where we have taken the SM value of γ as input. It is evident that the QCD penguins for $\pi\pi$, πK, and KK follow a pattern:

$$|P| \lesssim |P'| \lesssim |P''|, \tag{29}$$

and roughly agree with a factorization based estimation in that the SU(3) breaking effects are proportional to the decay constants of the final states, namely.

$$\frac{P'}{P} \approx \frac{P''}{P'} \approx \frac{f_K}{f_\pi}. \tag{30}$$

Thus one finds that a separate analysis can indeed provide important information on decay amplitudes and test SU(3) symmetry breaking, which cannot be obtained by a global χ^2 analysis.

IV. ANALYSIS USING FLAVOR SU(3) SYMMETRY

A. Fit within SM

We are in the position now to connect the $\pi\pi$, πK, and KK modes through approximate flavor SU(3) symmetry. Note that there is no reliable way to estimate the size of the SU(3) breaking in theory. From the factorization based approaches the SU(3) breaks in such a way that the amplitudes in the $\pi K(KK)$ modes differ from the ones in the $\pi\pi(\pi K)$ modes by a factor of f_K/f_π, where f_K and f_π are decay constants for K and π mesons. There have been analyses based on different patterns of SU(3) breaking which could in general lead to different results. Here we would like to consider three scenarios of SU(3) relations frequently used in the literature:

Scenario A.—All diagrammatic amplitudes for $\pi K(KK)$ modes are larger than that in $\pi\pi(\pi K)$ modes by a factor f_K/f_π,

$$\frac{T'}{T} = \frac{C'}{C} = \frac{P'}{P} \cdots = \frac{T''}{T'} = \frac{C''}{C'} = \frac{P''}{P'} \cdots = \frac{f_K}{f_\pi}. \tag{31}$$

Scenario B.—SU(3) symmetry breaks only in tree diagrams [41,42]

$$\frac{T'}{T} = \frac{T''}{T'} = \frac{f_K}{f_\pi}, \qquad \frac{C'}{C} = \frac{P'}{P} \cdots = \frac{C''}{C'} = \frac{P''}{P'} \cdots = 1. \tag{32}$$

Scenario C.—Exact SU(3) limit

$$\frac{T'}{T} = \frac{C'}{C} = \frac{P'}{P} \cdots = \frac{T''}{T'} = \frac{C''}{C'} = \frac{P''}{P'} \cdots = 1. \tag{33}$$

As in the first step, the $P_{\rm EW}$ is fixed within the SM through Eq. (5). Thus there are 6 parameters T, C, δ_C, P, δ_P, and γ to be fitted by 18 data points. The best-fit parameters as well as the Brs and a_{CP}s are tabulated in Table II.

The results show that:

(i) The differences among the three scenarios are in general not large. The weak phase γ is well determined in all the cases and depends on the SU(3) breaking scheme very weakly. All three scenarios give $\gamma \simeq 1.1$ in good agreement with the SM value with differences less than 10%, which manifests that γ can be reliably extracted using the diagrammatic approach. The $\chi^2_{\rm min}$ curves as a function of γ are given in Fig. 2. Comparing with the one from the $\pi\pi$ fit, one finds a significant improvement on the precision of γ determination. The three patterns lead to roughly the same $|T|$ and $|C|$ with $|C/T| \simeq 0.8$. Note that for small $|C|$ we find no consistent fit. For example, if $|C|$ is fixed at $C = 0.2$, a very big $\chi^2_{\rm min}/\text{d.o.f.} = 44.6/12$ is obtained. The major difference is the value of $|P|$. Scenarios B and C prefer a $|P|$ which is $\sim$20% larger.

TABLE II. Global fit to $\pi\pi$, πK, and KK modes within the SM. The three columns corresponds to the three different SU(3) relations used in the fits.

	Scenario A	Scenario B	Scenario C
$\lvert T\rvert$	0.52 ± 0.027	0.51 ± 0.033	0.52 ± 0.032
$\lvert C\rvert$	0.47 ± 0.042	0.45 ± 0.053	0.45 ± 0.053
δ_C	-1.1 ± 0.19	$-1^{+0.21}_{-0.19}$	$-1.1^{+0.21}_{-0.19}$
$\lvert P\rvert$	0.094 ± 0.0014	0.12 ± 0.0019	0.12 ± 0.0018
δ_P	$-0.49^{+0.089}_{-0.1}$	$-0.45^{+0.087}_{-0.11}$	$-0.54^{+0.11}_{-0.13}$
$\lvert P_{\rm EW}\rvert$	0.011 ± 0.0011	0.011 ± 0.0011	0.011 ± 0.0011
$\delta_{P_{\rm EW}}$	-0.52 ± 0.1	-0.47 ± 0.11	-0.49 ± 0.11
γ	$1^{+0.11}_{-0.13}$	$1.1^{+0.13}_{-0.17}$	$1.1^{+0.14}_{-0.17}$
$\chi^2_{\rm min}$/d.o.f.	$16.2/12$	$19.2/12$	$21/12$
$\mathrm{Br}(\pi^+\pi^-)$	4.7 ± 0.48	4.8 ± 0.62	4.9 ± 0.59
$a_{CP}(\pi^+\pi^-)$	0.27 ± 0.062	0.32 ± 0.085	0.37 ± 0.096
$\mathrm{Br}(\pi^0\pi^0)$	1.7 ± 0.31	1.8 ± 0.4	1.8 ± 0.41
$a_{CP}(\pi^0\pi^0)$	0.36 ± 0.11	0.43 ± 0.15	0.38 ± 0.17
$\mathrm{Br}(\pi^-\pi^0)$	5.2 ± 0.77	5.1 ± 0.85	5.1 ± 0.86
$a_{CP}(\pi^-\pi^0)$	0 ± 0.01	0 ± 0.01	0 ± 0.01
$\mathrm{Br}(\pi^+K^-)$	20 ± 0.77	20 ± 0.84	20 ± 0.74
$a_{CP}(\pi^+K^-)$	-0.1 ± 0.02	-0.097 ± 0.022	-0.089 ± 0.019
$\mathrm{Br}(\pi^0\bar{K}^0)$	9.8 ± 0.49	9.9 ± 0.47	9.7 ± 0.46
$a_{CP}(\pi^0\bar{K}^0)$	-0.1 ± 0.035	-0.076 ± 0.03	-0.068 ± 0.032
$\mathrm{Br}(\pi^-\bar{K}^0)$	22 ± 0.69	22 ± 0.71	22 ± 0.68
$\mathrm{Br}(\pi^0K^-)$	12 ± 0.63	11 ± 0.64	12 ± 0.57
$a_{CP}(\pi^0K^-)$	0.0055 ± 0.042	-0.016 ± 0.039	-0.014 ± 0.04
$\mathrm{Br}(K^0\bar{K}^0)$	1.3 ± 0.17	2.3 ± 0.35	0.84 ± 0.13
$\mathrm{Br}(K^-\bar{K}^0)$	1.3 ± 0.17	2.3 ± 0.35	0.84 ± 0.13
$S(\pi^+\pi^-)$	-0.73 ± 0.13	-0.76 ± 0.13	-0.73 ± 0.14
$S(\pi^0\pi^0)$	0.23 ± 0.27	0.51 ± 0.27	0.52 ± 0.27
$S(\pi^0K_S)$	0.86 ± 0.038	0.84 ± 0.04	0.84 ± 0.04

(ii) Among the three cases, scenario A shows that all the primed (double-primed) amplitudes are larger than the unprimed (primed) ones by a factor of f_K/f_π, gaining the lowest $\chi^2/\text{d.o.f.} = 16.2/12$, which indicates a better consistency in comparison with the other two. The exact SU(3) scenario gains the largest $\chi^2/\text{d.o.f.} = 21/12$, which clearly indicates that the flavor SU(3) symmetry in charmless B decays must be a broken one.

(iii) The main source of the inconsistency comes from the $\mathrm{Br}(\pi^+K^-)$, $\mathrm{Br}(\pi^0\overline{K}^0)$, and $\mathrm{Br}(\pi^-\overline{K}^0)$. The best fits in scenario A prefer a larger $\mathrm{Br}(\pi^+K^-) \simeq 20$, a small $\mathrm{Br}(\pi^0\overline{K}^0) \simeq 9.8$, and a small $\mathrm{Br}(\pi^-\overline{K}^0) \simeq 22$. Namely, within the current parametrization, it is not possible to arrive at the observed ratios R_n and R. Thus the πK puzzles remain.

(iv) For the predictions for the KK modes, scenario A gives $\mathrm{Br}(K^0\bar{K}^0) = \mathrm{Br}(K^-\bar{K}^0) = 1.2$, while the other two give 1.7 (scenario B) and 0.84 (scenario C), respectively. The branching ratio of K^+K^- is predicted to be zero and all the predicted direct CP violations are vanishing, due to the lack of interferences between amplitudes.

Other possibilities of SU(3) breaking include the SU(3) breaking in strong phases, which has been discussed in Ref. [34]. The current data favor a small SU(3) breaking in the strong phase of the QCD penguin. This breaking effect can significantly modify the correlation of direct CP asymmetries between $\pi\pi$ and πK modes [2].

B. Fit with free electroweak penguin $P_{\rm EW}$

In the next step, we consider the possibility that $P_{\rm EW}$ is free from the SM constraint. The fitting results with free $P_{\rm EW}$ under three scenarios are given in Table III. The χ^2 curves are shown in Fig. 4.

In this case, one finds that all the fits prefer a larger value of $|P_{\rm EW}| = 0.23$–0.29 with a large strong phase $\delta_{P_{\rm EW}} = 0.6$–$0.7$ relative to $\hat{T}$ as the corresponding best fit of $\hat{T}$ has a strong phase of $-0.5 \sim -0.4$. A large $P_{\rm EW}$ with a large strong phase relative to $\hat{T}$ can naturally explain the suppression of R_n and also R_2 [2,18–20,36–39]. Naively speaking, all πK modes are QCD penguin dominant; the ratios R_n and R_2 should be very close to unity. The corrections arise from either tree-type diagrams or electroweak penguins. The former is CKM suppressed in πK modes and is constrained by $\pi\pi$ data. Thus an enhancement of the electroweak penguin is needed.

TABLE III. The same as Table II, but $P_{\rm EW}$ is taken as a free parameter to be determined directly from the data.

	Scenario A	Scenario B	Scenario C
$\lvert T\rvert$	0.52 ± 0.028	$0.51^{+0.037}_{-0.045}$	0.51 ± 0.035
$\lvert C\rvert$	0.45 ± 0.052	$0.44^{+0.096}_{-0.062}$	$0.44^{+0.078}_{-0.064}$
δ_C	$-0.96^{+0.23}_{-0.21}$	-0.92 ± 0.25	-0.98 ± 0.24
$\lvert P\rvert$	0.093 ± 0.0015	0.12 ± 0.0019	0.12 ± 0.0019
δ_P	$-0.52^{+0.1}_{-0.13}$	$-0.49^{+0.1}_{-0.24}$	$-0.59^{+0.13}_{-0.22}$
$\lvert P_{\rm EW}\rvert$	$0.023^{+0.0096}_{-0.011}$	0.027 ± 0.014	0.029 ± 0.013
$\delta_{P_{\rm EW}}$	$0.63^{+0.21}_{-0.41}$	$0.7^{+0.23}_{-0.35}$	$0.63^{+0.23}_{-0.32}$
γ	$1^{+0.13}_{-0.18}$	$1.1^{+0.16}_{-0.36}$	$1^{+0.17}_{-0.26}$
$\chi^2_{\rm min}$/d.o.f.	$13.2/10$	$15.9/10$	$18/10$
$\mathrm{Br}(\pi^+\pi^-)$	4.7 ± 0.53	4.8 ± 0.84	4.9 ± 0.7
$a_{CP}(\pi^+\pi^-)$	0.29 ± 0.077	0.34 ± 0.14	0.39 ± 0.14
$\mathrm{Br}(\pi^0\pi^0)$	1.6 ± 0.38	1.7 ± 0.66	1.7 ± 0.58
$a_{CP}(\pi^0\pi^0)$	0.14 ± 0.18	0.16 ± 0.26	0.12 ± 0.26
$\mathrm{Br}(\pi^-\pi^0)$	5.4 ± 0.89	5.3 ± 1.2	5.2 ± 1.1
$a_{CP}(\pi^-\pi^0)$	-0.085 ± 0.045	-0.11 ± 0.061	-0.11 ± 0.06
$\mathrm{Br}(\pi^+K^-)$	20 ± 0.85	20 ± 1.1	20 ± 0.84
$a_{CP}(\pi^+K^-)$	-0.11 ± 0.024	-0.1 ± 0.035	-0.093 ± 0.027
$\mathrm{Br}(\pi^0\bar{K}^0)$	11 ± 1.9	11 ± 1.8	11 ± 1.9
$a_{CP}(\pi^0\bar{K}^0)$	-0.034 ± 0.045	-0.027 ± 0.043	-0.02 ± 0.042
$\mathrm{Br}(\pi^-\bar{K}^0)$	22 ± 0.73	22 ± 0.74	22 ± 0.73
$\mathrm{Br}(\pi^0K^-)$	12 ± 2.2	12 ± 2.2	12 ± 2.2
$a_{CP}(\pi^0K^-)$	0.033 ± 0.059	0.012 ± 0.063	0.01 ± 0.057
$\mathrm{Br}(K^0\bar{K}^0)$	1.3 ± 0.21	2.3 ± 0.56	0.81 ± 0.17
$\mathrm{Br}(K^-\bar{K}^0)$	1.3 ± 0.21	2.3 ± 0.56	0.81 ± 0.17
$S(\pi^+\pi^-)$	-0.7 ± 0.17	-0.73 ± 0.22	-0.71 ± 0.2
$S(\pi^0\pi^0)$	0.4 ± 0.31	0.54 ± 0.41	0.55 ± 0.36
$S(\pi^0K_S)$	0.86 ± 0.039	0.84 ± 0.043	0.84 ± 0.042

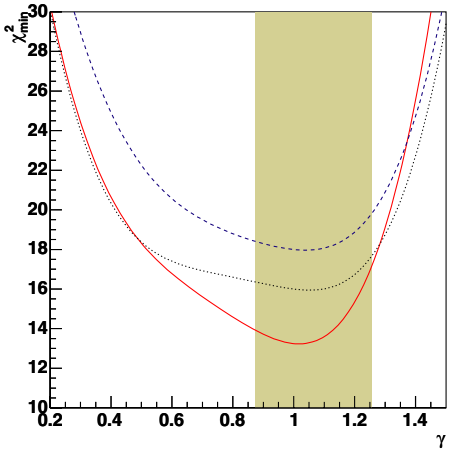

FIG. 4 (color online). $\chi^2_{\rm min}$ as functions of the weak phase γ. The three upper curves correspond to the three fits in Table III. The solid, dashed, and dotted curves correspond to scenarios A, B, and C, respectively. The shadowed band is the allowed range from the global SM fit.

As the two ratios R_n and R_2 are both $P_{\rm EW}$ sensitive, they can be used as probes of electroweak penguins. We parametrize the deviation of SM by introducing a complex parameter κ

$$\frac{\hat{P}_{\rm EW}}{\hat{T}} = R^{\rm SM}_{\rm EW} \cdot \kappa. \tag{34}$$

In Fig. 5, the two ratios are plotted with different values of $|\kappa|$ and its strong phase $\delta\kappa$. For demonstration reasons, the other parameters are fixed at the best-fit values in SM in the first column of Table II according to scenario A, namely,

$$\begin{aligned} &T = 0.52, \qquad C = 0.47, \qquad \delta_C = -1.1, \\ &P = 0.094, \quad \text{and} \quad \delta_P = -0.49. \end{aligned} \tag{35}$$

The figures indicate strong dependences on $\delta\kappa$ and $|\kappa|$ for both ratios. In the SM case, i.e., $|\kappa| = 1$ and $\delta_\kappa = 0$, R_n is expected to be above 1.0 in contrast with the experiment. For $|\kappa| = 1$ and large $\delta_\kappa \sim 1.5$, R_n is reduced but R_2 is enhanced and departs away from the allowed range of the data. Thus to simultaneously explain both measurements, one needs a large $|\kappa| \simeq 2.0$–3.0 and a large strong phase of $\delta_\kappa \simeq 1.0$–1.5. This observation is confirmed by the global fits with $P_{\rm EW}$ free in Table III which gives

$$\frac{P_{\rm EW}}{\hat{T}} = \begin{cases} (3.1 \pm 1.3)e^{i(1.02\pm0.5)} \times 10^{-2} & \text{(scenario A)}, \\ (4.8 \pm 1.5)e^{i(1.06\pm0.53)} \times 10^{-2} & \text{(scenario B)}, \\ (3.1 \pm 1.5)e^{i(1.03\pm0.5)} \times 10^{-2} & \text{(scenario C)}. \end{cases} \tag{36}$$

With $P_{\rm EW}$ being free , the best-fit $\pi^0\bar{K}^0$ mode is found to be $\mathrm{Br}(\pi^0\bar{K}^0) = 11 \pm 1.9$ in scenario A, in remarkable agreement with the data. The central values of the two ratios are found to be $R_n \simeq R_2 \simeq 0.9$.

The enhanced $P_{\rm EW}$ with a large strong phase will result in different predictions for the CP asymmetries. In most decay modes the predicted a_{CP}s are much smaller [2]. However, the most important one is $a_{CP}(\pi^-\pi^0)$ which should be exactly zero in SM. But now it prefers a negative value of $a_{CP}(\pi^-\pi^0) \sim -0.1$, which is in agreement with the current preliminary data of $a_{CP} = -0.02 \pm 0.07$ and can be examined with more precise data in the near future.

It needs to be emphasized that the *large* $P_{\rm EW}$ here means a relative enhancement to the tree-type diagram $\hat{T}$, not to the QCD penguin diagram. It was claimed recently in Ref. [13] that there was no clear indication of large $P_{\rm EW}/P$, which does not necessarily contradict with the conclusions in the present paper. Furthermore, using the numerical value of T and C obtained in Ref. [13], we find a similar result as in Eq. (36). Note that the ratio $P_{\rm EW}/P$ is subjected to large theoretical uncertainties. It is better to use the values relative to $\hat{T}$ for exploring the electroweak

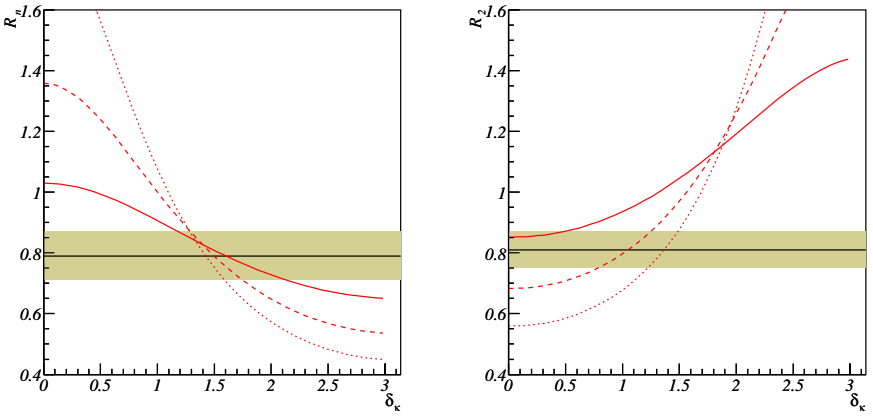

FIG. 5 (color online). R_n and R_2 as functions of δ_κ with a different value of $|\kappa|$. The three curves correspond to $|\kappa| = 1.0$, (solid), 2.0 (dashed), and 3.0 (dotted). The shadowed bands are the experimentally allowed ranges. Other parameters are fixed at the SM best-fit values (column A in Table II).

penguin and new physics as it is free from hadronic uncertainties.

C. Effects of color-suppressed electroweak penguin $P^C_{\rm EW}$

In the previous discussions, the color-suppressed electroweak penguin diagram $P^C_{\rm EW}$ is neglected. However, among all the subleading diagrams $P^C_{\rm EW}$ is the only one giving a contribution to the high isospin state $I = 2(3/2)$ in $\pi\pi$ (πK) modes. Furthermore, it cancels the isospin $I = 0(1/2)$ components of $P_{\rm EW}$ just like C cancels that of T and directly contributes to the ratio in Eq. (5). Since the current data indicate a sizable C, it is still possible that there will be an enhancement of $P^C_{\rm EW}$ as well. In the SM, $\hat{P}_{\rm EW}$ is fixed relative to $\hat{T}$. However, given a large relative strong phase, i.e., negative interference between $P_{\rm EW}$ and $P^C_{\rm EW}$, a large value of $P^C_{\rm EW}$ is possible within the SM. Note that the $\pi^0\bar{K}^0$ mode depends on $P_{\rm EW} + P^C_{\rm EW}/3 = \hat{P}_{\rm EW}/3 + 2P_{\rm EW}/3$. Even if the first term is constrained by Eq. (5), the second term can still enhance the decay rate of the $\pi^0\bar{K}^0$ mode without violating the SM relation. A similar argument also applies to $\pi^0 K^-$ modes which depends on $P_{\rm EW} + 2P^C_{\rm EW}/3$.

To see the effects of $P^C_{\rm EW}$, we give in Fig. 6 the ratios of R_n and R_2 as a function of $P^C_{\rm EW}$ and its strong phase $\delta_{P^C_{\rm EW}}$. In the numerical calculations we take the values of other amplitudes from the SM fit, according to the first column of Table II or Eq. (35). The values of $P_{\rm EW}$ and its strong phase are automatically generated from Eq. (5). It follows from the figure that for a small $|P^C_{\rm EW}| \simeq 0.1$ the predicted value of R_n is far above the data for all values of $\delta_{P^C_{\rm EW}}$. To account for the current data $|P^C_{\rm EW}|$ has to be greater than $\sim$0.4. The strong phase $\delta_{P^C_{\rm EW}}$ receives strong constraint from R_2. For $|P^C_{\rm EW}|$ in the range 0.1–0.6, a large negative value of $\delta_{P^C_{\rm EW}} = -0.2 \sim -2.5$ is favored.

Including $P^C_{\rm EW}$ as a new free parameter while keeping Eq. (5), we find

$$|P^C_{\rm EW}| = 0.025 \pm 0.021, \qquad \delta_{P^C_{\rm EW}} = -2.24^{+0.21}_{-0.63}, \quad (37)$$

and

$$|P_{\rm EW}| = 0.03^{+0.02}_{-0.013}, \qquad \delta_{P_{\rm EW}} = 0.52^{+0.31}_{-0.72}, \quad (38)$$

with a χ^2/d.o.f. $= 11.3/10$. The best fits of other parameters are listed in the first column of Table IV. Clearly, there is a strong cancellation in the sum of $P_{\rm EW} + P^C_{\rm EW}$ as required by Eq. (5). It is of interest to note that for both tree and penguin diagrams the color-suppressed diagrams are not necessarily suppressed. Furthermore, the current data suggest that

$$\left|\frac{C}{T}\right| \simeq \left|\frac{P^C_{\rm EW}}{P_{\rm EW}}\right| \approx 0.8. \quad (39)$$

Thus the relative enhancements are likely to be universal. This is again in favor of the conjecture that it has a strong interaction origin which is flavor independent. Comparing with Eq. (40), one sees that $P^C_{\rm EW}$ is on the lower side to account for the suppression of R_n. The best-fit ratios are $R_n \simeq 0.89$ and $R_2 \simeq 0.78$ respectively. Thus a large $P^C_{\rm EW}$ improves the agreement with the data.

Taking both $P_{\rm EW}$ and $P^C_{\rm EW}$ as independent free parameters, we get the following fit result:

$$|P^C_{\rm EW}| = 0.016 \pm 0.02, \qquad \delta_{P^C_{\rm EW}} = -2.59^{+0.4}_{-1.7}, \quad (40)$$

and

$$|P_{\rm EW}| = 0.027^{+0.016}_{-0.014}, \qquad \delta_{P_{\rm EW}} = 0.69^{+0.3}_{-0.6}, \quad (41)$$

with $\chi^2_{\rm min}$/d.o.f. $= 6.6/8$. The color-suppressed electroweak penguin is found to be reduced but still significant. In this case, all the πK ratios are well reproduced. Note that the best fits correspond to $|\hat{P}_{\rm EW}/\hat{T}| = 0.032 \pm 0.018$ which again implies a violation of the SM relation.

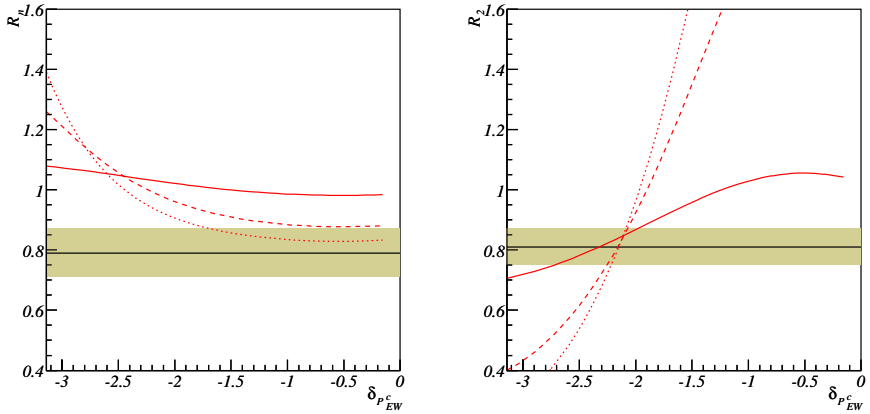

FIG. 6 (color online). Ratios of R and R_2 as functions of $\delta_{P^C_{\rm EW}}$ and $|P^C_{\rm EW}|$. The three curves correspond to $|P^C_{\rm EW}| = 0.01$ (solid), 0.04 (dashed), and 0.06 (dotted), respectively. Other parameters are fixed at their best-fit value in SM (according to column A of Table II). The shadowed bands are the allowed range by the current data.

TABLE IV. Global fits to $\pi\pi$, πK, and KK data with subleading diagrams. The four columns correspond to the four cases, where in each of them one subleading diagram is set to be free parameters.

	A	B	C	D
$\lvert T\rvert$	0.51 ± 0.027	$0.94^{+0.31}_{-0.24}$	0.53 ± 0.026	0.51 ± 0.027
$\lvert C\rvert$	0.47 ± 0.048	$0.26^{+0.2}_{-0.11}$	$0.48^{+0.1}_{-0.046}$	0.48 ± 0.044
δ_C	$-0.97^{+0.28}_{-0.22}$	$-2.1^{+0.83}_{-0.72}$	$-1.1^{+0.2}_{-0.55}$	$-1.1^{+0.2}_{-0.18}$
$\lvert P\rvert$	$0.094^{+0.0018}_{-0.0021}$	0.097 ± 0.0022	0.094 ± 0.0015	0.093 ± 0.0015
δ_P	-0.41 ± 0.14	$-0.26^{+0.087}_{-0.13}$	$-0.47^{+0.093}_{-0.11}$	$-0.54^{+0.1}_{-0.13}$
$\lvert P_{\rm EW}\rvert$	$0.03^{+0.019}_{-0.013}$	0.011 ± 0.0011	0.011 ± 0.0011	0.011 ± 0.0011
$\delta_{P_{\rm EW}}$	$0.52^{+0.31}_{-0.71}$	$-0.28^{+0.14}_{-0.16}$	$-0.54^{+0.11}_{-0.25}$	-0.53 ± 0.11
$\lvert P^C_{\rm EW}\rvert$	$0.025^{+0.018}_{-0.02}$	0 (fix)	0 (fix)	0 (fix)
$\delta_{P^C_{\rm EW}}$	$-2.24^{+0.21}_{-0.61}$	0 (fix)	0 (fix)	0 (fix)
$\lvert E\rvert$	0 (fix)	$0.46^{+0.26}_{-0.31}$	0 (fix)	0 (fix)
δ_E	0 (fix)	$2.86^{+0.17}_{-0.23}$	0 (fix)	0 (fix)
$\lvert P_A\rvert$	0 (fix)	0 (fix)	$0.035^{+0.026}_{-0.15}$	0 (fix)
δ_{P_A}	0 (fix)	0 (fix)	-2.26 ± 0.48	0 (fix)
$\lvert A\rvert$	0 (fix)	0 (fix)	0 (fix)	$0.23^{+0.12}_{-0.087}$
δ_A	0 (fix)	0 (fix)	0 (fix)	$2.77^{+0.28}_{-0.35}$
γ	$0.93^{+0.13}_{-0.16}$	$0.94^{+0.12}_{-0.15}$	$0.93^{+0.13}_{-0.43}$	$0.93^{+0.12}_{-0.15}$
$\chi^2_{\rm min}$/d.o.f.	11.3/10	13.2/10	14.3/10	13.8/10

Finally, we emphasize that the large $P^C_{\rm EW}$ within the SM may distinguish itself from the one beyond the SM by the prediction of direct CP violation in $B \to \pi^-\pi^0$ which should be vanishing in the former case and small but nonzero in the latter.

Given a small $P^C_{\rm EW}$ relative to $P_{\rm EW}$, the current data may imply new physics beyond the SM. New physics models significantly contributing to charmless B decays may include various supersymmetric models [22], Z' models from extra U(1) gauge symmetry [21,59], and two-Higgs-doublet models (2HDMs) [60]. Among various versions of two-Higgs-doublet models, the general 2HDM with spontaneous CP violation can provide rich sources of CP violation [61–65] and significant corrections to the electroweak penguin through charge or neutral-Higgs boson exchanges. The models with the 4th generation may also give sizable contributions. For models with both two-Higgs-doublet and 4th generation quarks, the effects could be more significant through neutral-Higgs loops [66–68].

V. NONFACTORIZABLE DIAGRAMS

We now go a step further to discuss the effects of other subleading nonfactorizable diagrams such as E, A, and P_A. They are expected to be very small from factorization based estimations. However, in the presence of large FSI, there could be mixing among diagrams which may enhance the sizes of subleading diagrams [25–27]. In view of the current puzzling pattern of the data, the possibility of anomalously large nonfactorizable diagrams cannot be excluded [69].

Because of the limited number of data points, it is not possible to directly extract all of them simultaneously from the current data of $\pi\pi$, πK, and KK. Instead, to obtain the typical sizes of those diagrams, we shall consider several typical cases; in each case only one of the diagrams is assumed to be dominant while the other two are small. For simplicity, we consider only the case where $P_{\rm EW}$ is fixed as the SM value.

A. W-exchange diagram E

It has been argued that sizable E with constructive (destructive) interference with $C(T)$ can help to understand the large value of $|C/T|$ obtained when E is absent [18–20]. The main contribution to $\pi^+\pi^-$ is from $T + E$ while it is $C - E$ for the $\pi^0\pi^0$ mode. To illustrate how E improves the consistency with the $\pi\pi$ data with a small $|C/T|$, we fix the tree and color-suppressed tree to be

$$|T| = 0.9, \qquad |C| = 0.3, \quad \text{and} \quad \delta_C = 0, \tag{42}$$

respectively. The QCD penguin is fixed at $|P| = 0.1$, $\delta_P = -0.5$ and $P_{\rm EW}$ is fixed at its SM value. In this case, the dependence of R_{00} and R_{+-} with E and its strong phase δ_E is plotted in Fig. 7

As shown in the figure, for a small ratio of $|C/T| = 0.3$, the data require a large $|E| \simeq 0.3$–0.5 with a large strong phase of ~ 2.0. However, The origin of large E is still a challenge for theory.

Assuming E is dominant, we find a big value from a fit to the data

$$|E| = 0.46^{+0.26}_{-0.31}, \qquad \delta_E = 2.86^{+0.17}_{-0.23}. \tag{43}$$

The whole fit result is given in column B of Table IV. The $\chi^2_{\rm min}$/d.o.f. is 13.2/10. Note that although $|C/T|$ is reduced to ~ 0.28, the relative strong phase δ_C is found to be large

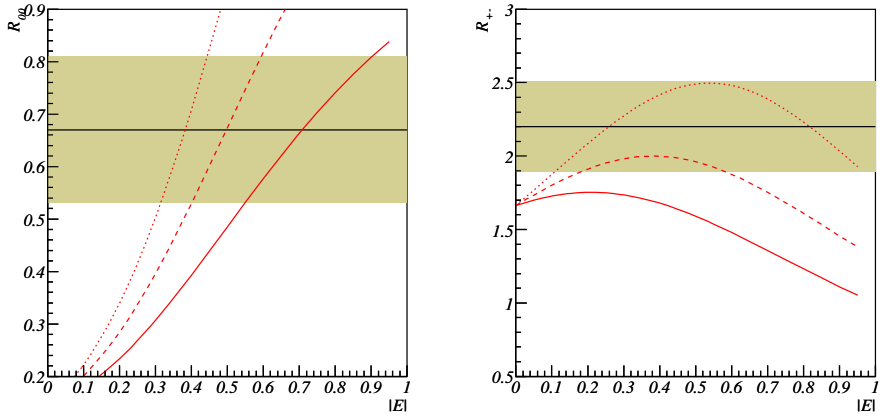

FIG. 7 (color online). R_{00} and R_{+-} as functions of E with different values of δ_E The three curves correspond to $\delta_E = 1.8$ (solid), 2.0 (dashed), and 2.2 (dotted). The shadowed bands are the experimentally 1σ allowed ranges.

$\delta_C = -2.1^{+0.83}_{-0.72}$ in contradiction with factorization based estimates. Thus only introducing a large W-exchange diagram will not be enough to coincide with factorization results.

An alternative way to reduce C/T is to make P_{tu} significantly different than P or P_{tc}. This is less likely as P_u is greatly suppressed relative to P_t by a small u-quark mass in the Wilson coefficient. The important FSI process such as a charming penguin affects only P_{tc}. A fit taking P_{tu} and P_{tc} as independent parameters shows that the best-fit P_{tc} is close to the factorization estimate of P while P_{tu} is large and compatible with T in size [42], which is quite unreasonable.

As mentioned previously, an enhanced E has no effect in the πK modes, thus it cannot solve the πK puzzle and explain the obtained large C'/T'. The best-fit branching ratios in πK still exhibit the puzzling patterns.

B. Annihilation diagram A

The annihilation diagram A appears in $\pi^-\overline{K}^0$ and $\pi^0 K^-$ modes. The current data indicate that both of them are large in comparison with the $\pi^+ K^-$ mode, which is characterized by the suppression of R_2 and R. This may imply a sizable A in these modes as discussed in the previous sections. In Fig. 8 the two ratios are given as functions of A and δ_A. The other parameters are fixed at the SM best-fit value in Table II.

One sees from the figure that the two ratios have a similar behavior under the changing of A and δ_A. For A ranges between 0.3–0.8, both ratios decrease with δ_A growing. For $|A| = 0.5$–0.8 the curves fall down to the experimentally allowed ranges at $\delta_A > 2.0$. Since both ratios contain the same term $\mathcal{A} + \mathcal{P}$, they have similar dependences on A and δ_A. This will lead to a cancellation for the ratio of the ratios: $R/R_2 = 2\mathrm{Br}(\pi^0 K^-)/\mathrm{Br}(\pi^-\bar{K}^0)$ should be very close to unity, which agrees with the data well.

Assuming A is dominant over other subleading diagrams and using scenario A for SU(3) breaking, we find

$$|A| = 0.23^{+0.12}_{-0.09}, \qquad \delta_A = 2.77^{+0.28}_{-0.35}, \tag{44}$$

with $\chi^2_{\min}/\mathrm{d.o.f.} = 13.8/10$. The whole fitting results are listed in column D of Table IV. One sees that the best-fit value of A is moderate, which helps to reduce R and R_2 but is not large enough to reproduce the central values of the two ratios. Note that even this value of $|A| \sim 0.2$ is still much larger than that from the factorization estimation which is suppressed by a factor of f_B/m_B.

C. Penguin-annihilation diagram P_A

In the $\pi\pi$ modes, the penguin-induced annihilation diagram P_A contributes to only low isospin final states ($I = 0$) and it always comes together with QCD penguin P in $\pi\pi$ modes. Although P_A is often neglected in the literature, its effects are however effectively absorbed into the QCD penguin in the $\pi\pi$ modes. Thus the QCD penguins extracted from the $\pi\pi$ modes are effectively $\tilde{P} = P + P_A$. In general P_A acquires a strong phase different than that of P, namely, the strong phases of $\tilde{P}$ and P are different. Since there is no SU(3) counterpart P'_A appearing in πK modes, P' is still have the same strong phase as that of P in SU(3) symmetry. This introduces an effective SU(3) breaking in strong phase between $\tilde{P}$ extracted from the $\pi\pi$ modes and P' from πK. A fit to the current data gives the following values:

$$P_A = 0.035^{+0.026}_{-0.015}, \qquad \delta_{P_A} = -2.26 \pm 0.48. \tag{45}$$

Thus its size is compatible with that of the electroweak penguin. The $\chi^2_{\min}/\mathrm{d.o.f.}$ is found to be $14.3/10$. The other best-fit parameters can be found in column C of Table IV. The best-fit value corresponds to $\tilde{P} \simeq 0.093$ and $\delta_{\tilde{P}} \simeq -0.85$, which corresponds to a strong phase shift of

$$\Delta\delta_P = \delta'_P - \delta_{\tilde{P}} \simeq 0.38. \tag{46}$$

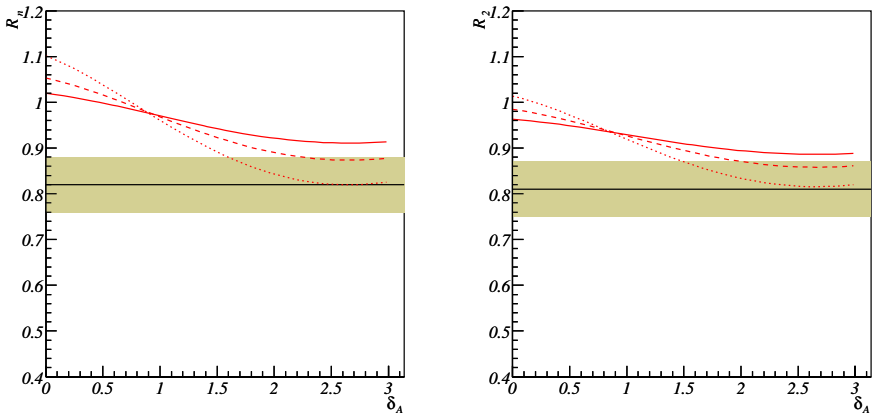

FIG. 8 (color online). R and R_2 as functions of δ_A with different values of A. The three curves correspond to $A = 0.3$ (solid), 0.5 (dashed), and 0.8 (dotted). The shadowed bands are the experimentally allowed ranges.

This is in good agreement with the previous analyses in Refs. [2,34].

VI. IMPLICATIONS FOR KK MODES

The KK modes are much more sensitive to the subleading diagrams $\mathcal{E}$, $\mathcal{A}$, and $\mathcal{P}_A$. The $K^0\bar{K}^0$ mode is dominated by the QCD penguin as discussed in Sec. III. The decay amplitudes of the other two modes read

$$\begin{aligned}\bar{\mathcal{A}}(K^+K^-) &= -[\lambda_u(E'' - P_A'') - \lambda_c P_A''],\\ \bar{\mathcal{A}}(K^-\bar{K}^0) &= \lambda_u\left(-P'' + \frac{1}{3}P_{\mathrm{EW}}^{C''} + A''\right)\\ &\quad - \lambda_c\left(P'' - \frac{1}{3}P_{\mathrm{EW}}^{C''}\right).\end{aligned} \tag{47}$$

The K^+K^- modes depend only on the subleading diagrams E and P_A. Thus it provides an ideal avenue to explore their effects. From the current upper bound of $\mathrm{Br}(K^+K^-) \lesssim 1.8$ [28], and the SU(3) relation of scenario A, the exchanging diagram E receives a constraint of

$$|E| \lesssim 0.3, \tag{48}$$

which limits its contribution to the $\pi\pi$ modes to be moderate as the best fit to the $\pi\pi$ modes requires $|E| \approx 0.48$ in Eq. (43). It is expected that a stronger constraint on E will be found with more precise data in the near future.

The direct CP violations for K^+K^- and $K^-\bar{K}^0$ read

$$a_{CP}(K^+K^-) = \frac{2|\lambda_u\lambda_c||P_A''E''|\sin\gamma\sin\delta}{|\lambda_u|^2(|E''|^2 + |P_A''|^2 - 2|P_A''E''|\cos\delta) + |\lambda_c|^2|P_A''|^2 + 2|\lambda_u\lambda_c||P_A''|\cos\gamma(|E''|\cos\delta - |P_A''|)}, \tag{49}$$

and

$$a_{CP}(K^-\bar{K}^0) \simeq \frac{2|\lambda_u\lambda_c||P''A''|\sin\gamma\sin\delta'}{|\lambda_u|^2(|A''|^2 + |P''|^2 - 2|A''P''|\cos\delta') + |\lambda_c|^2|P''|^2 + 2|\lambda_u\lambda_c||P''|\cos\gamma(|A''|\cos\delta' - |P''|)}, \tag{50}$$

where $\delta = \delta_{P_A''} - \delta_{E''}$ and $\delta' = \delta_{P''} - \delta_{A''}$. In the expression of $a_{CP}(K^-\bar{K}^0)$ the color-suppressed electroweak penguins are neglected. A nonzero $a_{CP}(K^+K^-)$ will definitely indicate both nonzero E and P_A. In spite of the small branching ratio, in the case that E and P_A are compatible in size, and the strong phase difference is large, then the direct CP violation could be significant.

Unlike in the πK modes where A is suppressed by a factor $|\lambda_u^s/\lambda_c^s| = \mathcal{O}(\lambda^2)$, in the $K^-\bar{K}^0$ mode, it is not suppressed. Thus it is promising to probe A in the $K^-\bar{K}^0$ mode. A sizable annihilation diagram A will show up either through the difference between $\mathrm{Br}(K^0\bar{K}^0)$ and $\mathrm{Br}(K^-\bar{K}^0)$ or through the nonzero direct CP violation, i.e., $a_{CP}(K^-\bar{K}^0) \neq 0$.

In Fig. 9, the decay rate and direct CP violation of the $K^-\bar{K}^0$ mode are plotted as a function of A. In the numerical calculations, the values of A'' and P'' are calculated from the best-fit value of P according to scenario A. For δ_A in the range 0–2.5, both decay rate and direct CP violation increase with A increasing. One sees from the figure that for $|A| = 0.15$–0.2 and $\delta_A = 2.5$–3.0, $a_{CP}(K^-\bar{K}^0)$ can reach 0.2–0.4 with the branching ratio in agreement with the current data. Thus with significantly large subleading diagrams, it is promising to observe large direct CP violation in this decay mode.

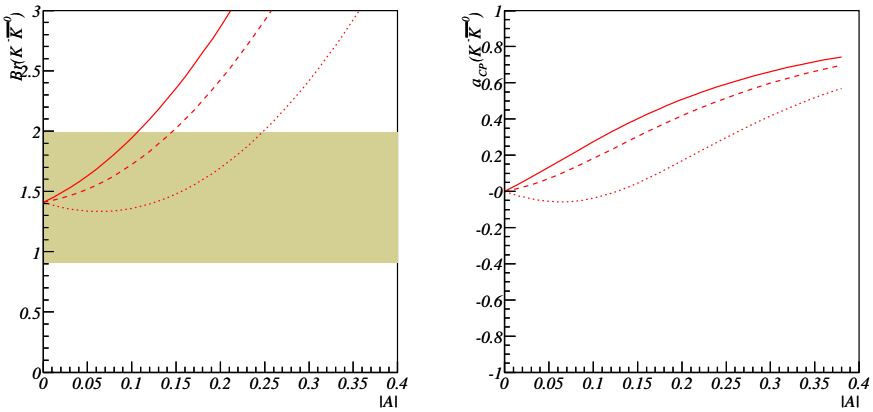

FIG. 9 (color online). Branching ratio and direct CP violation of $K^-\bar{K}^0$ as functions of A with different values of δ_A. The three curves correspond to $\delta_A = 0$ (solid), 2.5 (dashed), and 3.0 (dotted), respectively. The shadowed band is the experimentally 1σ allowed range. Other parameters are fixed at their best-fit value in the SM (according to column A of Table II). The SU(3) breaking effects are taken into account according to scenario A.

VII. SUMMARY

In summary, we have systematically studied charmless B decays $B \to \pi\pi$, πK, and KK, following a strategy making an independent analysis for $\pi\pi$, πK, KK modes individually as the first step and then connecting them through various SU(3) relations. The separated analysis allowed us to clarify the origins of the inconsistency or puzzles revealed by the current data. Independent analyses on $\pi\pi$ and πK modes *both* favor a large ratio of C/T and C'/T' with large strong phases, which suggests that they are more likely to originate from long distance strong interactions rather than large nonfactorizable exchange diagrams E. The sizes of QCD penguin diagrams in $\pi\pi$, πK, and KK are independently extracted and were found to follow a pattern of SU(3) breaking in good agreement with factorization estimation $P'/P \simeq P''/P' \simeq f_K/f_\pi$. Global fits to these modes have been carried out under various scenarios of SU(3) relations. All results show good determinations of weak phase γ in consistency with the SM and prefer a large electroweak penguin ($P_{\rm EW}$) relative to $T + C$ with a large strong phase. Within the SM, it may require an enhancement of color-suppressed electroweak penguin ($P^C_{\rm EW}$) with destructive interference to $P_{\rm EW}$. The possibility of the presence of new physics effects cannot be excluded. We have also investigated the possibility of sizable contributions from nonfactorizable diagrams such as E, A, and P_A. Their sizes could be significantly larger than the expected ones. The typical sizes of $|E|$ could reach to $|E| \approx 0.3$ as required by the $\pi\pi$ and KK data, $|A|$ could reach to $|A| \approx 0.2$ while $|P_A|$ has a typical value of $|P_A| \approx 0.03$. The sizable subleading diagrams may change significantly the predictions for the yet to be seen K^+K^- and $K^-\bar{K}^0$ modes. The CP violation in the $K^-\bar{K}^0$ modes could reach $a_{CP} \simeq 0.2 \sim 0.4$ for a large value of A and δ_A in the range of $|A| = 0.15$–0.2 and $\delta_A = 2.5$–2.5. It would be encouraging to expand the investigation of subleading diagrams to decay modes involving η and η' final states. Although these decay modes receive significant contributions from additional flavor singlet penguin diagrams [70–73] or nonstandard contributions through $\bar{c}c$ [74,75] or QCD anomaly [76,77], as more data points are involved, stronger constraints on the subleading diagrams will be expected. Thus it will enable us to test the SM using the full diagrammatic decomposition.

ACKNOWLEDGMENTS

Y. L. W. is supported in part by the key project of NSFC and the Chinese Academy of Sciences. Y. F. Z. is grateful to S. Safir for reading the manuscript and for useful comments.

[1] K. Abe *et al.* (Belle Collaboration), Phys. Rev. D **68**, 012001 (2003); B. Aubert *et al.* (*BABAR* Collaboration), Phys. Rev. Lett. **93**, 131801 (2004); Z. Ligeti, in *Proceedings of ICHEP04, Beijing, 2004* (World Scientific, Singapore, 2004); M. Giorgi, *ibid.*, hep-ex/0408113; Y. Sakai, *ibid.*, hep-ex/0410006.

[2] Y.-L. Wu and Y.-F. Zhou, Phys. Rev. D **71**, 021701 (2005).

[3] Y.-Y. Keum, H.-n. Li, and A. I. Sanda, Phys. Lett. B **504**, 6 (2001).

[4] Y. Y. Keum and A. I. Sanda, Phys. Rev. D **67**, 054009 (2003).

[5] A. Ali and C. Greub, Phys. Rev. D **57**, 2996 (1998).

[6] A. Ali, G. Kramer, and C.-D. Lu, Phys. Rev. D **58**, 094009 (1998).
[7] M. Beneke and M. Neubert, Nucl. Phys. **B675**, 333 (2003).
[8] M. Beneke, G. Buchalla, M. Neubert, and C. T. Sachrajda, Phys. Rev. Lett. **83**, 1914 (1999).
[9] M. Beneke, G. Buchalla, M. Neubert, and C. T. Sachrajda, Nucl. Phys. **B591**, 313 (2000).
[10] M. Beneke, G. Buchalla, M. Neubert, and C. T. Sachrajda, Nucl. Phys. **B606**, 245 (2001).
[11] S. Barshay, G. Kreyerhoff, and L. M. Sehgal, Phys. Lett. B **595**, 318 (2004).
[12] X.-G. He and B. H. J. McKellar, hep-ph/0410098.
[13] Y.-Y. Charng and H.-n. Li, Phys. Rev. D **71**, 014036 (2005).
[14] H.-Y. Cheng, C.-K. Chua, and A. Soni, Phys. Rev. D **71**, 014030 (2005).
[15] T. Carruthers and B. H. J. McKellar, hep-ph/0412202.
[16] A. Ali, E. Lunghi, and A. Y. Parkhomenko, Eur. Phys. J. C **36**, 183 (2004).
[17] A. Y. Parkhomenko, hep-ph/0411061.
[18] A. J. Buras, R. Fleischer, S. Recksiegel, and F. Schwab, Phys. Rev. Lett. **92**, 101804 (2004).
[19] A. J. Buras, R. Fleischer, S. Recksiegel, and F. Schwab, Nucl. Phys. **B697**, 133 (2004).
[20] A. J. Buras, R. Fleischer, S. Recksiegel, and F. Schwab, Acta Phys. Pol. B **36**, 2015 (2005).
[21] V. Barger, C.-W. Chiang, P. Langacker, and H.-S. Lee, Phys. Lett. B **598**, 218 (2004).
[22] X.-G. He, C.-S. Li, and L.-L. Yang, Phys. Rev. D **71**, 054006 (2005).
[23] D. London, J. Matias, and J. Virto, Phys. Rev. D **71**, 014024 (2005).
[24] A. Datta *et al.*, Phys. Rev. D **71**, 096002 (2005).
[25] L. Wolfenstein, Phys. Rev. D **52**, 537 (1995).
[26] M. Neubert, Phys. Lett. B **424**, 152 (1998).
[27] J. M. Gerard and J. Weyers, Eur. Phys. J. C **7**, 1 (1999).
[28] For a summary, see Heavy Flavor Averaging Group, http://www.slac.stanford.edu/xorg/hfag/rare
[29] C. W. Bauer, I. Z. Rothstein, and I. W. Stewart, Phys. Rev. Lett. **94**, 231802 (2005).
[30] M. Neubert, J. High Energy Phys. 02 (1999) 014.
[31] Y. Grossman, M. Neubert, and A. L. Kagan, J. High Energy Phys. 10 (1999) 029.
[32] M. Gronau and J. L. Rosner, Phys. Lett. B **572**, 43 (2003).
[33] X.-G. He, Eur. Phys. J. C **9**, 443 (1999).
[34] Y. L. Wu and Y. F. Zhou, Eur. Phys. J. C **32**, 179 (2004).
[35] Y. F. Zhou, Y. L. Wu, J. N. Ng, and C. Q. Geng, Phys. Rev. D **63**, 054011 (2001).
[36] T. Yoshikawa, Phys. Rev. D **68**, 054023 (2003).
[37] D. Atwood and G. Hiller, hep-ph/0307251.
[38] S. Mishima and T. Yoshikawa, Phys. Rev. D **70**, 094024 (2004).
[39] S. Nandi and A. Kundu, hep-ph/0407061.
[40] X. G. He *et al.*, Phys. Rev. D **64**, 034002 (2001).
[41] C.-W. Chiang, M. Gronau, Z. Luo, J. L. Rosner, and D. A. Suprun, Phys. Rev. D **69**, 034001 (2004).
[42] C.-W. Chiang, M. Gronau, J. L. Rosner, and D. A. Suprun, Phys. Rev. D **70**, 034020 (2004).
[43] J. Charles *et al.* (CKMfitter Group), Eur. Phys. J. C **41**, 1 (2005).
[44] M. Bona *et al.* (UTfit Collaboration), J. High Energy Phys. 07 (2005) 028.
[45] M. Gronau, O. F. Hernandez, D. London, and J. L. Rosner, Phys. Rev. D **50**, 4529 (1994).
[46] M. Gronau, O. F. Hernandez, and D. London, Phys. Rev. D **52**, 6374 (1995).
[47] M. Gronau and J. L. Rosner, Phys. Rev. D **53**, 2516 (1996).
[48] B. Aubert *et al.* (*BABAR* Collaboration), Phys. Rev. Lett. **90**, 181801 (2003).
[49] S. B. Athar *et al.* (CLEO Collaboration), Phys. Rev. D **68**, 072003 (2003).
[50] S. Hashimoto, A. S. Kronfeld, P. B. Mackenzie, S. M. Ryan, and J. N. Simone, Phys. Rev. D **66**, 014503 (2002).
[51] B. Aubert *et al.* (*BABAR* Collaboration), Phys. Rev. Lett. **94**, 161803 (2005).
[52] K. Abe *et al.* (Belle Collaboration), Phys. Rev. D **71**, 072003 (2005); **71**, 079903 (2005).
[53] M. Ciuchini, E. Franco, G. Martinelli, and L. Silvestrini, Nucl. Phys. **B501**, 271 (1997).
[54] M. Ciuchini, E. Franco, G. Martinelli, M. Pierini, and L. Silvestrini, Phys. Lett. B **515**, 33 (2001).
[55] C. Isola, M. Ladisa, G. Nardulli, T. N. Pham, and P. Santorelli, Phys. Rev. D **64**, 014029 (2001).
[56] C. Isola, M. Ladisa, G. Nardulli, T. N. Pham, and P. Santorelli, Phys. Rev. D **65**, 094005 (2002).
[57] Y.-L. Wu and Y.-F. Zhou, Phys. Rev. D **62**, 036007 (2000).
[58] S. Baek, P. Hamel, D. London, A. Datta, and D. A. Suprun, Phys. Rev. D **71**, 057502 (2005).
[59] X.-G. He, C.-L. Hsueh, and J.-Q. Shi, Phys. Rev. Lett. **84**, 18 (2000).
[60] Z.-j. Xiao, K.-T. Chao, and C. S. Li, Phys. Rev. D **65**, 114021 (2002).
[61] Y. L. Wu and L. Wolfenstein, Phys. Rev. Lett. **73**, 1762 (1994).
[62] L. Wolfenstein and Y. L. Wu, Phys. Rev. Lett. **73**, 2809 (1994).
[63] Y. L. Wu and Y. F. Zhou, Phys. Rev. D **61**, 096001 (2000).
[64] Y.-F. Zhou and Y.-L. Wu, Mod. Phys. Lett. A **15**, 185 (2000).
[65] Y.-L. Wu and Y.-F. Zhou, Phys. Rev. D **64**, 115018 (2001).
[66] Y.-L. Wu, Chin. Phys. Lett. **16**, 339 (1999).
[67] Y.-L. Wu and Y.-F. Zhou, Eur. Phys. J. C **36**, 89 (2004).
[68] Y.-L. Wu and Y.-F. Zhou, hep-ph/0501142.
[69] T. Feldman and T. Hurth, J. High Energy Phys. 11 (2004) 037.
[70] M. Gronau and J. L. Rosner, Phys. Rev. D **53**, 2516 (1996).
[71] A. S. Dighe, M. Gronau, and J. L. Rosner, Phys. Lett. B **367**, 357 (1996); **377**, 325(E) (1996).
[72] A. S. Dighe, M. Gronau, and J. L. Rosner, Phys. Rev. Lett. **79**, 4333 (1997).
[73] C.-W. Chiang and J. L. Rosner, Phys. Rev. D **65**, 074035 (2002); **68**, 039902(E) (2003).
[74] I. E. Halperin and A. Zhitnitsky, Phys. Rev. D **56**, 7247 (1997).
[75] I. E. Halperin and A. Zhitnitsky, Phys. Rev. Lett. **80**, 438 (1998).
[76] H. Fritzsch, Phys. Lett. B **415**, 83 (1997).
[77] H. Fritzsch and Y.-F. Zhou, Phys. Rev. D **68**, 034015 (2003).